Biomech Model Mechanobiol (2012) 11:677–688
DOI 10.1007/s10237-011-0342-y

ORIGINAL PAPER

Mathematical model and numerical simulation of the cell growth in scaffolds

Darae Jeong · Ana Yun · Junseok Kim

Received: 19 January 2011 / Accepted: 29 July 2011 / Published online: 10 August 2011

Abstract A scaffold is a three-dimensional matrix that provides a structural base to fill tissue lesion and provides cells with a suitable environment for proliferation and differentiation. Cell-seeded scaffolds can be implanted immediately or be cultured *in vitro* for a period of time before implantation. To obtain uniform cell growth throughout the entire volume of the scaffolds, an optimal strategy on cell seeding into scaffolds is important. We propose an efficient and accurate numerical scheme for a mathematical model to predict the growth and distribution of cells in scaffolds. The proposed numerical algorithm is a hybrid method which uses both finite difference approximations and analytic closed-form solutions. The effects of each parameter in the mathematical model are numerically investigated. Moreover, we propose an optimization algorithm which finds the best set of model parameters that minimize a discrete l_2 error between numerical and experimental data. Using the mathematical model and its efficient and accurate numerical simulations, we could interpret experimental results and identify dominating mechanisms.

Keywords Scaffolds · Numerical simulation · Multigrid · Cell growth · Cell mobility

1 Introduction

Tissue engineering covers a broad field that applies the principles of engineering and life sciences to develop the biological substitutes for restoring, maintaining or improving tissue or organ functions (Yang et al. 2001a; Nerem and Sambanis 1995; Skalak and Fox 1988; Lanza et al. 2000). One of the principle methods behind tissue engineering involves growing the relevant cells *in vitro* into the required three-dimensional organ or tissue. Three-dimensional tissues can be achieved by seeding the cells onto porous matrices, known as scaffolds, to which the cells attach and colonize for proliferation and differentiation within a suitable environment (Langer and Vacanti 1993; Hori et al. 2004). Therefore, scaffolds of different shapes, structure, and materials have been realized and studied (Eisenbarth 2007; Patel and Fisher 2008; Flaibani et al. 2010).

In designing scaffolds for tissue regeneration, special characteristics such as biological and mechanical requirements should be considered. The designed scaffold must facilitate cell attachment, growth of tissue, and the transport of nutrients and it must provide structural support of tissue regeneration (Fang et al. 2005). The methods for investigating mechanical properties of porous scaffolds were primarily based on using experimental approaches (Hing et al. 1999; Bose et al. 2002) and the finite element numerical analysis (Beaupr and Hayes 1985; Williams and Lewis 1982; Cahill et al. 2009). Moreover, a computer-aided characteristic approach was presented by Fang et al. (2005) and Flaibani et al. (2010). A fully three-dimensional structural approach was used for computer simulation of tissue differentiation (Nishimura et al. 2003). And another fully three-dimensional approach to bone regeneration in scaffolds was developed using porosity, Young's modulus, and dissolution rate of scaffolds (Byrne et al. 2007).

In constructing scaffolds, efficient cell seeding process primarily influences the overall performance of the resultant tissue-engineered constructs (Li et al. 2001; Yang et al. 2001b). Since mathematical models for cell growth in scaffolds are useful *in vitro* tools for interpreting experimental

D. Jeong · A. Yun · J. Kim (✉)
Department of Mathematics, Korea University,
Seoul 136-701, Republic of Korea
e-mail: cfdkim@korea.ac.kr
URL: http://math.korea.ac.kr/∼cfdkim

results, identifying the dominating mechanisms, and understanding the biological phenomena (Galban and Locke 1999), we need to set up mathematical models and design their accurate numerical methods to systematically investigate optimal seeding strategies.

For the individual cell growth, using a multiphase porous mixture theory for each component of the tissue, a mathematical model has been developed (Lemon et al. 2006). For the collective behavior of a large number of cells, cellular automata techniques were used (Longo et al. 2004; Ermentrout and Edelstein-Keshet 1993). Moreover, the evolution of cell density depending on spatial and temporal grids was mathematically modeled by a reaction–diffusion system (Murray 2002). Malda et al. (2004) developed a mathematical model for oxygen gradient calculations in a three-dimensional polymeric scaffold and compared simulation results with experimental data. Pisu et al. (2004) took into account suitable population balances to describe nutrients and cell density with respect to time and space. Considering the nutrients as oxygen, Obradovic et al. (2000) demonstrated development of spatial tissue heterogeneities in scaffolds for cell densities. However, interaction between nutrients and cell distributions for spatial and temporal predictions has comparably studied little, it needs to be studied more experimentally and mathematically (Lewis et al. 2005).

In this paper, we focus on a mathematical model considering nutrient diffusion and cell proliferation inside scaffolds. This mathematical model has been developed and simulated (Landman and Cai 2007; Dunn et al. 2006; Lewis et al. 2005). Lewis et al. (2005) developed a mathematical model in one-dimensional coordinate system and the predictions were compared with experimental data of Malda et al. (2004). In Dunn et al. (2006), using experimental measurements, *in vitro* cell growth in three-dimensional scaffolds was simulated with the initial cell seedings such as all seeding and alternating seeding. The cell density profile from experimental data was generally in good agreement with simulation of cell growth based on the mathematical model. However, there was some discrepancy between the numerical simulation results and experiment data of cell distribution in the scaffolds. To overcome this, we shall consider cell migration in our model which was suggested in Dunn et al. (2006) for the possible discrepancy. Moreover, we shall keep the time evolution for the nutrient concentration whereas a quasi-steady state was assumed in Dunn et al. (2006).

Our primary aim of this paper is to develop an efficient and accurate numerical scheme to find optimal model parameters to match simulation results with experimental data in cell growth in scaffolds. The paper is organized as follows. The governing equations are presented in Sect. 2. We propose a hybrid numerical method in Sect. 3. In Sect. 4, we present several numerical results in order to investigate effects of each model parameter. Finally, conclusions are derived in Sect. 5.

2 Governing equations

In this section, we derive a cell growth equation and a nutrient concentration equation in a scaffold. Let $U(\mathbf{x}, t)$ and $C(\mathbf{x}, t)$ be the cell density [cell/mL] and the nutrient concentration [mole/mL] in scaffolds, respectively. Here, the space coordinate $\mathbf{x} = (x, y, z)$ is in domain $\Omega = (0, L_x) \times (0, L_y) \times (0, L_z)$ and t denotes time.

The growth of cells in scaffolds can be modeled using a modified logistic growth law (Lewis et al. 2005). The cell growth rate depends on the cell density U and also on the nutrient concentration C. The cell grows until the cell density reaches the carrying capacity $U_{\max}$ [cell/mL]. We assume that cell migration is a random process and its dynamics is modeled by a diffusion term with the cell mobility M[cm^2/s]. Therefore, the cell growth equation is given by

$$\frac{\partial U(\mathbf{x}, t)}{\partial t} = M \triangle U(\mathbf{x}, t) + \lambda C(\mathbf{x}, t) U(\mathbf{x}, t) \left(1 - \frac{U(\mathbf{x}, t)}{U_{\max}}\right), \tag{1}$$

where λ is the kinetic constant for the specific rate of cell growth [mL/(s mole)].

The nutrient concentration follows the diffusion equation (Galban and Locke 1997; Lewis et al. 2005) with a constant diffusion coefficient. The nutrient concentration diffuses across the scaffold with a diffusion coefficient D[cm^2/s] and is consumed by cells with the specific consumption rate of the nutrient V [mL/(s cell)]. The nutrient concentration equation is given by

$$\frac{\partial C(\mathbf{x}, t)}{\partial t} = D \triangle C(\mathbf{x}, t) - V C(\mathbf{x}, t) U(\mathbf{x}, t). \tag{2}$$

The governing equations are an extension of the previous model by Dunn et al. (2006). The difference is that we include diffusion term in the cell growth equation to investigate the effect of cell mobility. We note that we do not consider the cell death in this modeling approach.

The approximated parameter values are as follows: The diffusion coefficient for the nutrient concentration is $D = 2 \times 10^{-5}$ cm^2/s, the dissolved nutrient concentration in the bulk fluid is $C_0 = 10^2$ nmole/mL, the consumption rate is $V = 10^{-8}$ mL/(s cell), and the maximal cell density is $U_{\max} = 10^7$ cells/mL. In the experiment, each scaffold was seeded with 1×10^5 MC3T3 cells in 100 μL of α-minimum essential medium. For more details about experimental scaffold fabrication, processing of histology, cell culture, and tissue culture system, see Dunn et al. (2006).

Now, we introduce dimensionless variables $C' = C/C_0$, $U' = U/U_{\max}$, $M' = M/M_0$, $x' = x/L$, $y' = y/L$,

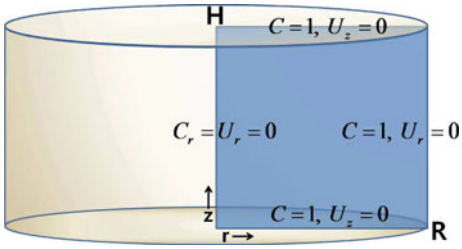

Fig. 1 *Shaded region* is the computational domain with the axisymmetric system

$$
\begin{array}{l}
(C^n, U^n) \\
\quad\downarrow \quad C_t = K\triangle C \text{ (multigrid method)} \\
(C^*, U^n) \\
\quad\downarrow \quad C_t = -RCU \text{ (analytic solution)} \\
(C^{n+1}, U^n) \\
\quad\downarrow \quad U_t = M\triangle U \text{ (multigrid method)} \\
(C^{n+1}, U^*) \\
\quad\downarrow \quad U_t = CU(1-U) \text{ (analytic solution)} \\
(C^{n+1}, U^{n+1})
\end{array}
$$

Fig. 2 A hybrid numerical method

$z' = z/L$, and $t' = t/T$, where $L = \sqrt{D/(VU_{\mathrm{m}})}$, $T = 1/(\lambda C_0)$, and $M_0 = L^2/T$. In typical cells, the growth rate λC_0 is 1/day. Thus, $T =$ one day. With these values, a characteristic length scale L is 140 μm and $M_0 = 2.3\times10^{-9}$ cm^2/s.

Then, Eq. (2) is replaced by nondimensional variables.

$$\frac{C_0\partial C'}{T\partial t'} = \frac{DC_0}{L^2}\triangle' C' - C_0 U_{\max} V C' U'.$$

After canceling out and changing variables, we obtain

$$\frac{\partial C'}{\partial t'} = K\triangle' C' - RC'U', \tag{3}$$

where two nondimensional values are defined as $K = TD/L^2$ and $R = TVU_{\max}$. Also, we have the following equation for the cell growth.

$$\frac{U_{\max}}{T}\frac{\partial U'}{\partial t'} = \lambda C' C_0 U' U_{\max}\left(1 - \frac{U_{\max}U'}{U_{\max}}\right) + M_0 M' \frac{U_{\max}\Delta U'}{L^2},$$

then,

$$\frac{\partial U'}{\partial t'} = M'\Delta U' + C'U'(1-U'). \tag{4}$$

After dropping primes, Eqs. (3) and (4) can be written as

$$\frac{\partial C}{\partial t} = K\triangle C - RCU, \tag{5}$$

$$\frac{\partial U}{\partial t} = M\triangle U + CU(1-U). \tag{6}$$

The initial conditions of C and U are $C(x, y, z, 0) = 1$ and $U(x, y, z, 0) = U_0/U_{\max}$, where U_0 is the initial cell density. The system of partial differential equations (5) and

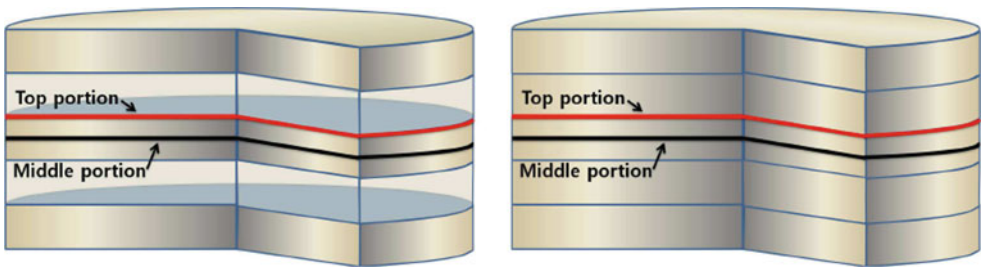

(a) Contstruct A **(b)** Contstruct B

Fig. 3 Stacking initial seeding patterns for constructs, A (alternating seeded slices) and B (uniform seeded slices)

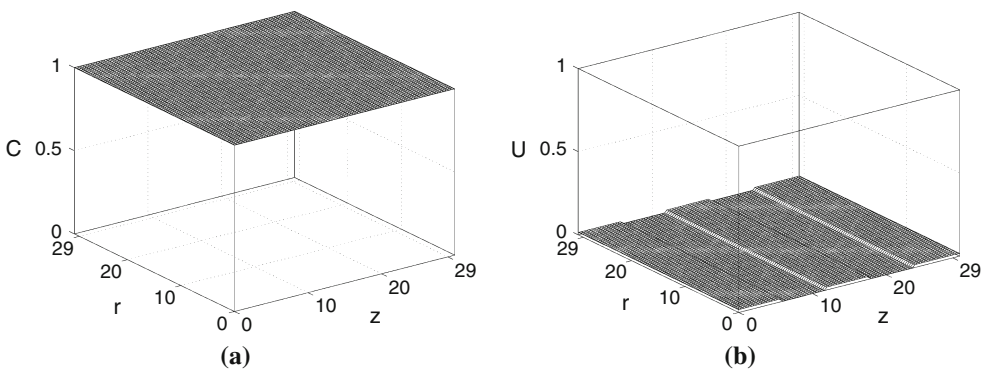

Fig. 4 Initial conditions of concentration and cell density. **a** $C(r, z, 0) = 1$ and **b** $U(r, z, 0) = 0.016$ on the first, the third, and the fifth scaffolds

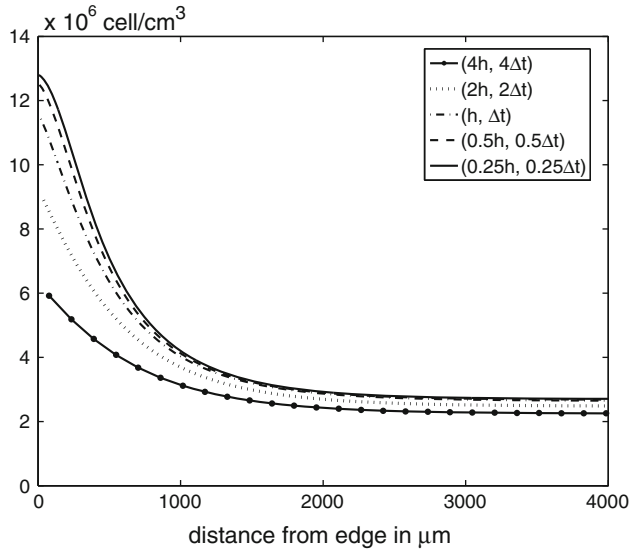

Fig. 5 Numerical results of cell density on top portion of the third scaffold at $T = 10$ with spatial and temporal grid refinements

(6) are solved in the axisymmetric $(r - z)$ geometry. Therefore, we consider only two variables; r is the radial direction and z is the axial direction. The governing equations in the axisymmetric geometry are expressed as

$$\frac{\partial C}{\partial t} = K\left[\frac{1}{r}(rC_r)_r + C_{zz}\right] - RCU, \tag{7}$$

$$\frac{\partial U}{\partial t} = M\left[\frac{1}{r}(rU_r)_r + U_{zz}\right] + CU(1-U). \tag{8}$$

In Fig. 1, the shaded region shows the computational domain with the axisymmetric system.

The boundary conditions are as follows. Due to the symmetry at the column axis $r = 0$, the Neumann boundary conditions are applied, i.e., $C_r(0, z, t) = 0, \quad U_r(0, z, t) = 0$. We assume the nutrient concentration is constant in the exterior of the scaffold. Therefore, at the rigid wall $r = R$, $C(R, z, t) = 1, \ U_r(R, z, t) = 0$, where R is the radius of the domain. At the top and bottom of the scaffold, the boundary conditions are $C(r, 0, t) = C(r, H, t) = 1, \ U_z(r, 0, t) = U_z(r, H, t) = 0$, where H is the height of the domain.

3 Numerical solution

We solve governing equations using a finite difference scheme depending both on spatially and temporally. The nutrient concentration C and the cell density U are defined on cell-centered grids. Let us first discretize the given computational domain $\Omega = (0, R) \times (0, H)$ as a uniform grid with a space step $h = R/N_r = H/N_z$ and a time step $\Delta t = T/N_t$. Let us denote the numerical approximations of the solution by

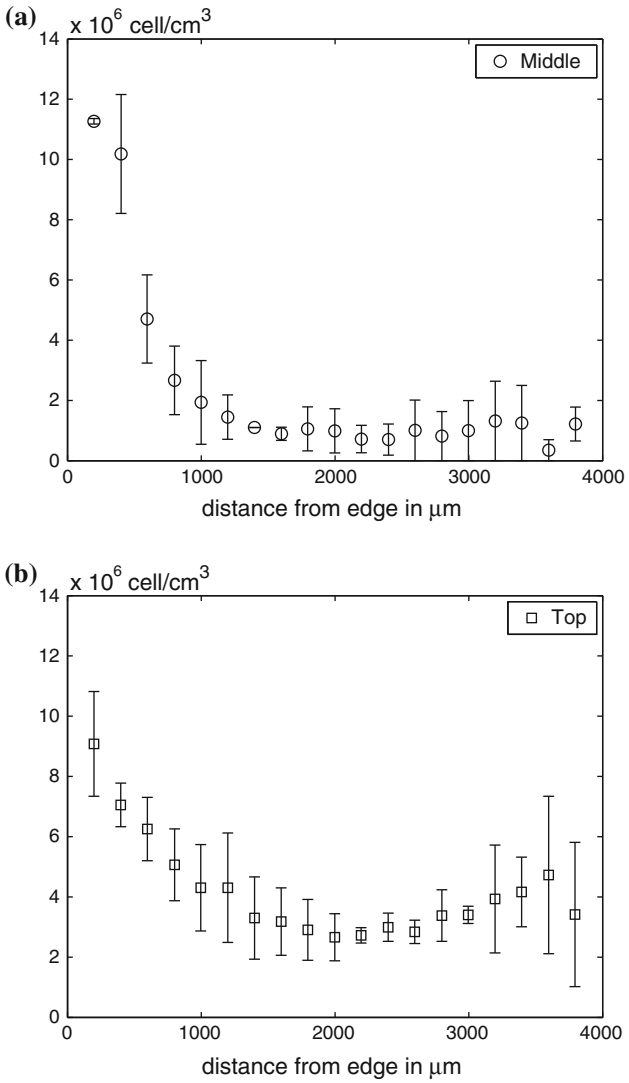

Fig. 6 Measured cell density for **a** middle (*circled*) and **b** top (*squared*) portions of the third scaffold in construct A on day 10. *Error bar* represents the standard deviation of measured cell density

$$C^n_{ik} \equiv C(r_i, z_k, t_n) = C\left((i-0.5)h, (k-0.5)h, n\Delta t\right),$$
$$U^n_{ik} \equiv U(r_i, z_k, t_n) = U\left((i-0.5)h, (k-0.5)h, n\Delta t\right),$$

where $i = 1, \ldots, N_r, \ k = 1, \ldots, N_z$, and $n = 0, \ldots, N_t$. Here, N_r, N_z, and N_t are the number of cells in r, z, and t directions, respectively.

In this paper, we propose an operator splitting method for governing Eqs. (7) and (8). The basic idea of this method is to split the original problem into a sequence of simpler problems.

Step 1 We solve implicitly the first part in Eq. (7) by a multigrid method (Briggs 1987; Trottenberg et al. 2001).

$$\frac{C^*_{ik} - C^n_{ik}}{\Delta t} = K\triangle_h C^*_{ik} = \frac{K}{h^2}\left[\frac{r_{i+\frac{1}{2},k}}{r_{ik}}\left(C^*_{i+1,k} - C^*_{ik}\right)\right.$$
$$\left. - \frac{r_{i-\frac{1}{2},k}}{r_{ik}}\left(C^*_{ik} - C^*_{i-1,k}\right) + C^*_{i,k-1} - 2C^*_{ik} + C^*_{i,k+1}\right].$$

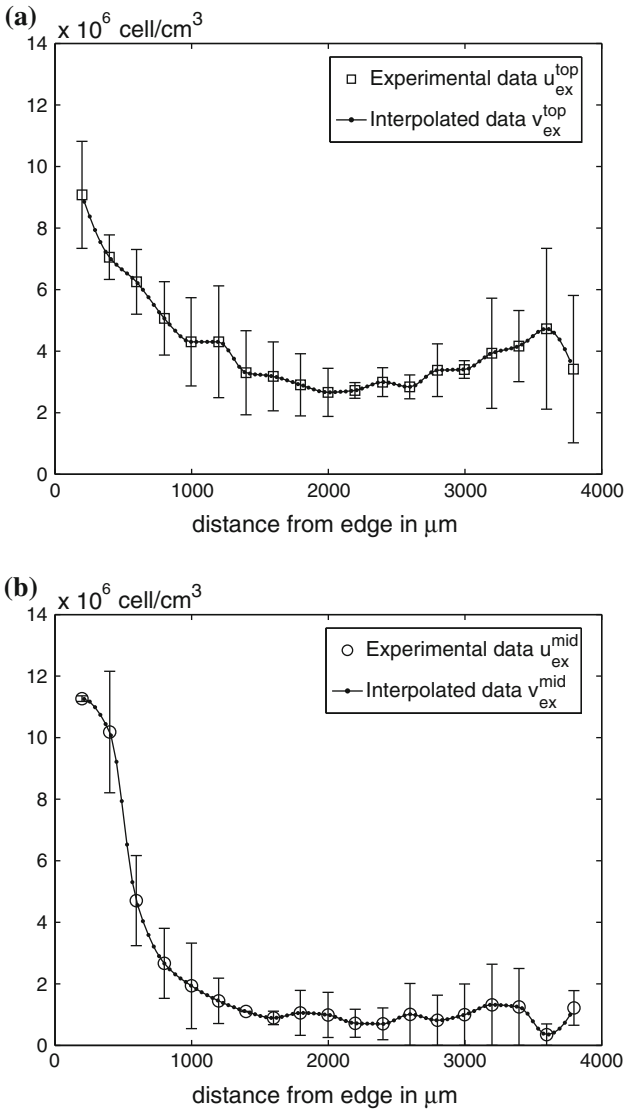

Fig. 7 Measured experimental data of cell density in the third stack of construct A on day 10 and shape-preserving interpolated data at each numerical grid point by experimental data. Here, **a** middle portion and **b** top portion

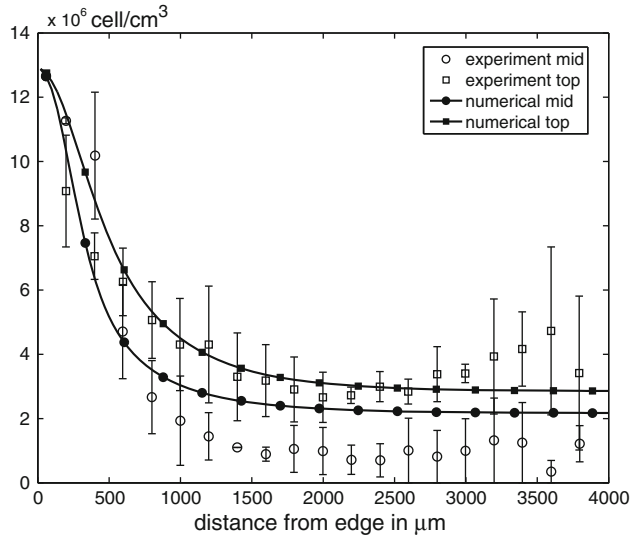

Fig. 8 Measured and simulated cell densities for the third scaffold in construct A. Middle portion (*circled line*) and top portion (*squared line*). *Error bar* represents the standard deviation of measured cell density. Numerical simulation were done with $K = 9.17$, $R = 11.44$, $M = 0$, $\Delta t = 0.01$, and $T = 10$

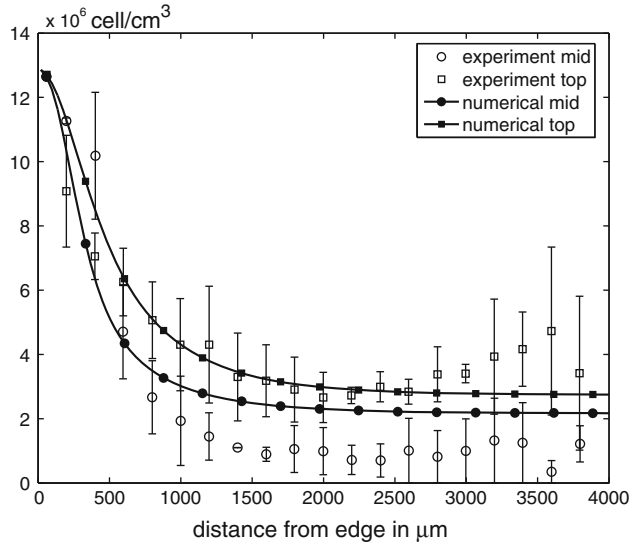

Fig. 9 Measured and simulated cell densities for the third scaffold in construct A. Middle portion (*circled line*) and top portion (*squared line*). *Error bar* represents the standard deviation of measured cell density. Numerical simulation were done with $K = 9$, $R = 11$, $M = 0.002$, $\Delta t = 0.01$, $T = 10$

Step 2 Then, the remaining term $\partial C/\partial t = -RCU$ in Eq. (7) is solved analytically by the method of separation of variables (Stuart and Humphries 1998) and the solution is given as

$$C_{ik}^{n+1} = C_{ik}^{*} e^{-\Delta t R U_{ik}^{n}}.$$

Step 3 We solve implicitly the first term in Eq. (8) using a multigrid method.

$$\frac{U_{ik}^{*} - U_{ik}^{n}}{\Delta t} = M \triangle_h U_{ik}^{*}.$$

Step 4 We solve the second equation $\partial U/\partial t = CU(1-U)$ in Eq. (8) analytically by the method of separation of variables and the solution is given as

$$U_{ik}^{n+1} = \frac{U_{ik}^{*}}{U_{ik}^{*} + \left(1 - U_{ik}^{*}\right) e^{-\Delta t C_{ik}^{n+1}}}.$$

In summary, our proposed numerical scheme to the system of Eqs. (7) and (8) consists of *Steps 1*, *2*, *3*, and *4*. Figure 2 shows our proposed numerical algorithm schematically.

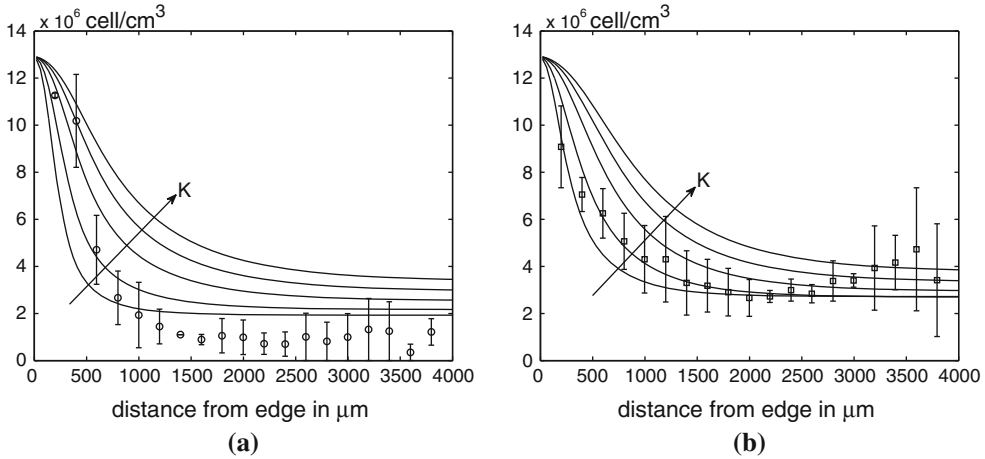

Fig. 10 Effect of varying the diffusivity of the nutrient concentration. The cell density for **a** the middle portion and **b** the top portion with $K = 4.5,\ 9,\ 18,\ 27$, and 36

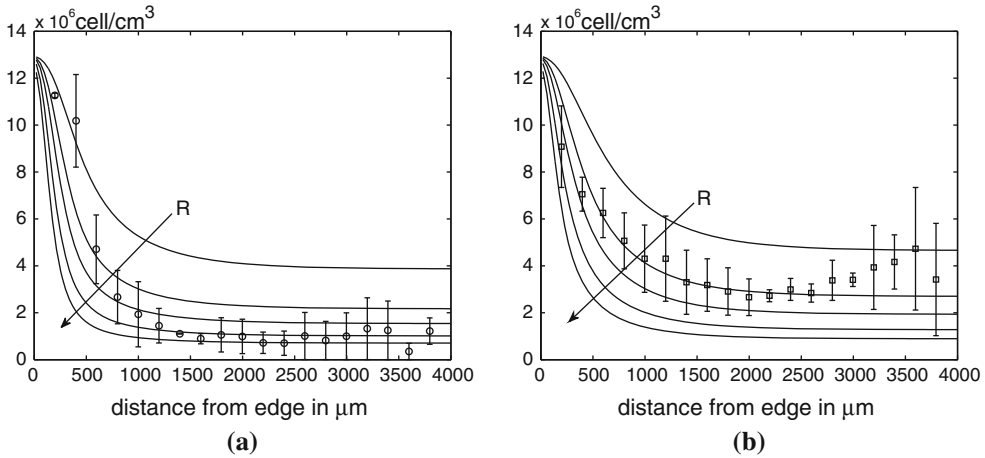

Fig. 11 Effect of varying the consumption rate of the nutrient on the cell density. The cell density for **a** the middle portion and **b** the top portion with $R = 5.5,\ 11,\ 16.5,\ 27.5$, and 44

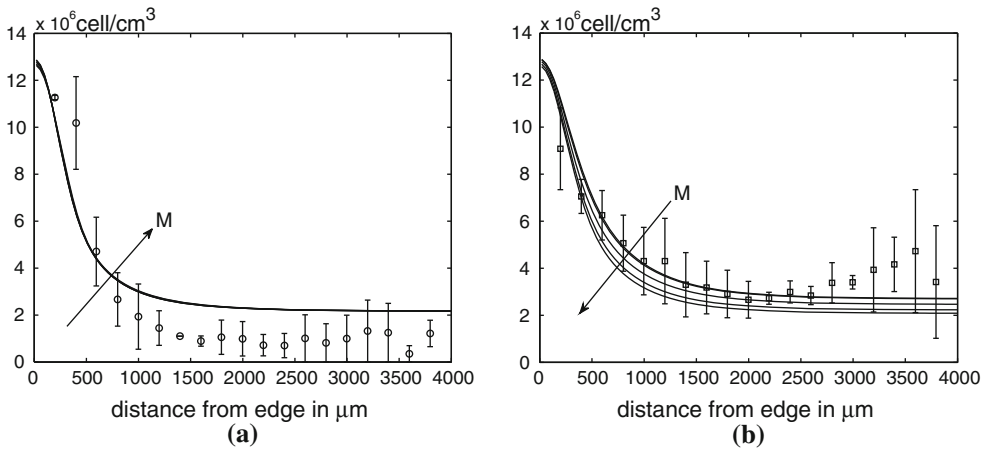

Fig. 12 Effect of varying the cell mobility. The cell density for **a** the middle portion and **b** the top portion with $M = 0, 0.002, 0.01, 0.02$, and 0.03

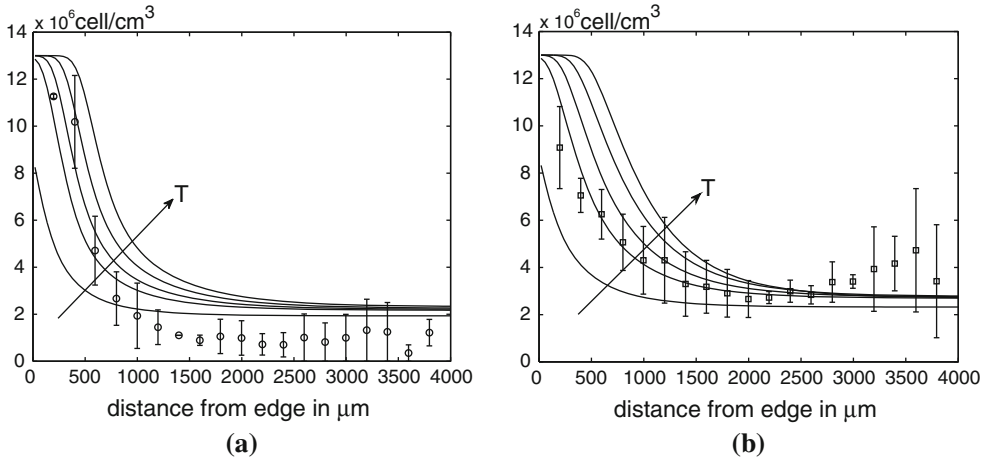

Fig. 13 Effect of varying the value of the time scale. The cell density for **a** the middle portion and **b** the top portion with $T = 5,\ 10,\ 15,\ 25,$ and 50

4 Computational results

In this section, we perform several numerical experiments such as convergence test, effects of each model parameter, and comparison with experimental data. Scaffolds are stacked in two initial seeding patterns as shown in Fig. 3. Construct A (Fig. 3a) contains five, stacked scaffolds, alternating between cell-seeded and unseeded. Construct B (Fig. 3b) contains five all cell-seeded scaffolds.

As the cell growth depends on the nutrient concentration, and the highest source of nutrients is at the scaffold interface, the growth of cells would be faster at the interface than inside the scaffold (Galban and Locke 1999). We use the experimental data from Dunn et al. (2006) for the initial conditions to compare numerical results. Figure 6 shows measured cell density for middle (circled line) and top (squared line) portions of the third scaffold in construct A on day 10. Error bar represents the standard deviation of measured cell density. This result shows higher cell density toward to the core of scaffolds in the top portions than the middle on the third scaffold. To find the optimal model parameters matching the experimental data, we focus on the region around 1,000–4,000 μm from the scaffold edge.

4.1 Convergence test

To confirm that our proposed numerical scheme is convergent, we perform a number of simulations with a set of increasingly finer spatial and temporal grids. We compute the numerical solutions on uniform grids, $4h$, $2h$, h, $h/2$, and $h/4$. For each case, we run the calculation up to time $T = 10$ with time steps $4\Delta t$, $2\Delta t$, Δt, $\Delta t/2$, and $\Delta t/4$. Time step $\Delta t = 0.1$ and space step $h = 1/128$ are used. The following parameters are used: $K = 9$, $R = 11$, and $M = 0.002$. In this paper, we take $L = 167$ μm for all numerical experiments. The initial conditions are $C(r, z, 0) = 1$ and $U(r, z, 0) = 0.016$ on the first, the third, and the fifth scaffolds (see Fig. 4).

Figure 5 shows the result of convergence test and we can confirm that the proposed scheme converges with respect to spatial and temporal refinements.

4.2 Optimal model parameter estimation

To estimate an optimal model parameter set, we propose a simple numerical algorithm. For simplicity of exposition, we will describe the algorithm with $M = 0$. With nonzero M, the algorithm can be similarly defined. The numerical algorithm consists of the following steps:

Step 1 First, we interpolate experimental data at numerical grid points r_i from Fig. 6 by using shape-preserving piecewise cubic hermite interpolation (Fritsch and Carlson 1980). Let $u_{\text{ex}}^{\text{mid}}$ and $u_{\text{ex}}^{\text{top}}$ be the original experimental data at middle and top portions in the third scaffold and $v_{\text{ex}}^{\text{mid}}$ and $v_{\text{ex}}^{\text{top}}$ be the corresponding interpolated data at grid points r_i (see Fig. 7).

Step 2 Choose initial guess for K and R. We solve Eqs. (7) and (8) using the proposed hybrid numerical method described in Sect. 3 with $0.9K$, K, $1.1K$ and $0.9R$, R, $1.1R$. This will result in nine numerical solutions with different K and R values. Among these results, we choose a parameter set which minimizes l_2-norm of error between experimental and numerical data. Then, we repeat this procedure until there is no change in the minimizing parameter set.

The details of overall steps are given in **Algorithm 1**.

Figure 8 shows measured and simulated cell densities for the third scaffold in construct A using **Algorithm 1**. The algorithm returns an optimal model parameter set, $K = 9.17$

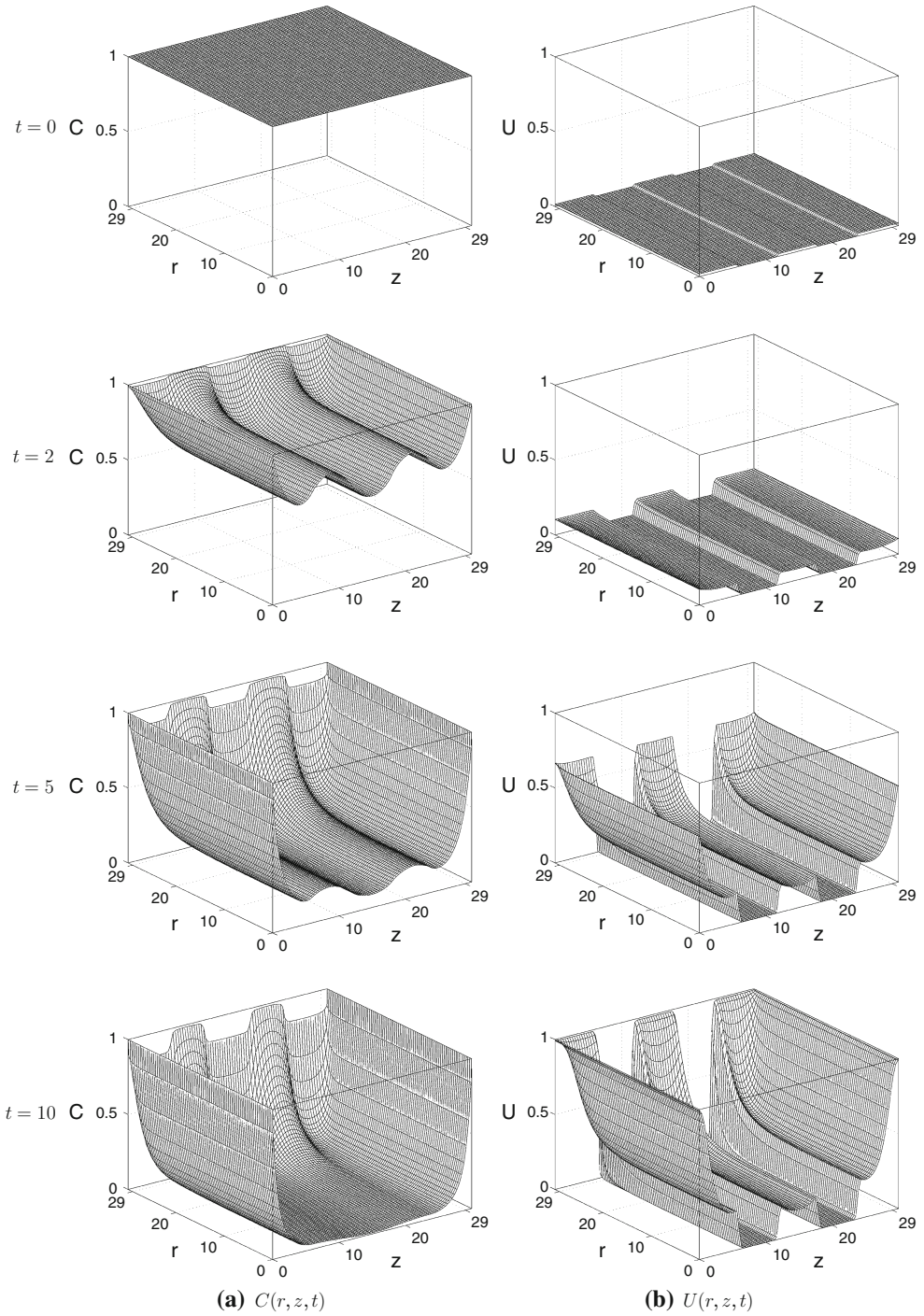

Fig. 14 The time evolution of the numerical solutions, **a** C and **b** U with $K = 9$, $R = 11$, $M = 0.002$, $\Delta t = 0.01$, and 256×256 mesh

and $R = 11.44$ with $M = 0$. A circled line (middle portion) and squared line (top portion) are numerical results. From the experimental data, the cell density in the top portion of the third scaffold is slightly higher than that in the middle portion of the third scaffold.

Next, we include nonzero M values in our algorithm and Fig. 9 shows measured and simulated cell densities for the third scaffold in construct A using **Algorithm 1**. The algorithm returns an optimal model parameter set, $K = 9$, $R = 11$, and $M = 0.002$. A circled line (middle portion) and squared line (top portion) are numerical results. From the experimental data, the cell density in the top portion of the third scaffold is slightly higher than that in the middle portion of the third scaffold.

Algorithm 1 Estimation of optimal model parameter

Require: Interpolated data $v_{\text{ex}}^{\text{mid}}, v_{\text{ex}}^{\text{top}}$ from experimental data $u_{\text{ex}}^{\text{mid}}, u_{\text{ex}}^{\text{top}}$.
procedure FIND OPTIMAL PARAMETER($testK, testR$)
  $testK = 50$ and $testR = 50$ ▷ Initial guess for K and R
  $\delta = 1.0E + 10$ ▷ Arbitrary large value
  $\Delta t = 0.01, T = 10, N_r = N_z = 128, itmax = T/\Delta t$
  repeat
    $\overline{K} = testK, \overline{R} = testR$
    for $k = 1; k \le 3; k{+}{+}$ **do**
      for $r = 1; r \le 3; r{+}{+}$ **do**
        $K = (0.8 + 0.1k)\overline{K}$ ▷ Parameter setting
        $R = (0.8 + 0.1r)\overline{R}$
        for $t = 1; t \le itmax; t{+}{+}$ **do** ▷ Time loop
          Perform four steps of the hybrid method (see Fig. 2)
        end for
        $err^{\text{mid}} = \sqrt{\frac{1}{N}\sum_{i=1}^{N}\left(u_i^{\text{mid}} - v_{\text{ex},i}^{\text{mid}}\right)^2}$ ▷ Evaluate l_2-error
        $err^{\text{top}} = \sqrt{\frac{1}{N}\sum_{i=1}^{N}\left(u_i^{\text{top}} - v_{\text{ex},i}^{\text{top}}\right)^2}$
        $result = 0.5(err^{\text{mid}} + err^{\text{top}})$
        if $result < \delta$ **then** ▷ Find the smallest l_2-error
          $\delta = result, testK = K, testR = R$
        end if
      end for
    end for
  until $|testK - \overline{K}| \le 0.01\overline{K}$ and $|testR - \overline{R}| \le 0.01\overline{R}$
end procedure

4.3 Effects of model parameters

In this section, we investigate the effects of each model parameters.

4.3.1 Effect of K

In this model, K represents the diffusivity of the nutrient concentration. To investigate the effect of K, we perform several simulations with varying K values. Figure 10 shows the cell density for (a) the middle portion and (b) the top portion of the third scaffold with $K = 4.5,\ 9,\ 18,\ 27$, and 36. With increasing values of K, we can observe more cell densities deep inside the scaffolds at both middle and top portions.

4.3.2 Effect of R

R represents the consumption rate of the nutrient by the cell. Figure 11 shows the cell density for (a) the middle portion and (b) the top portion with $R = 5.5,\ 11,\ 16.5,\ 27.5$, and 44. With decreasing values of R, we observe higher cell densities in the top portion than the middle.

4.3.3 Effect of M

M represents the cell mobility. Figure 12 shows the cell density for (a) the middle portion and (b) the top portion with $M = 0, 0.002, 0.01, 0.02$, and 0.03. As we increase values of the mobility, the cell density at the top and the middle portions becomes uniform.

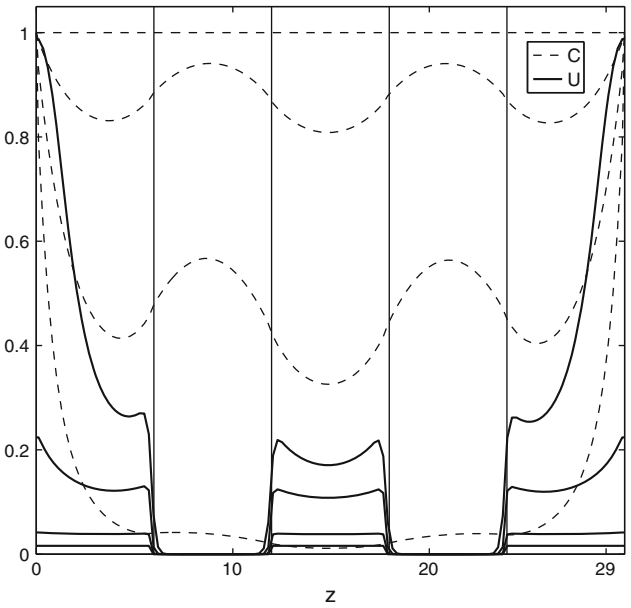

Fig. 15 Slice plot of nutrient concentration and cell density, C and U, at the axis of symmetry

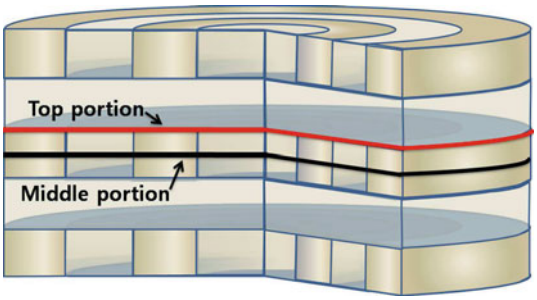

Fig. 16 Construct C

4.3.4 Effect of T

T represents the value of the time scale. Figure 13 shows the cell density for (a) the middle portion and (b) the top portion with $T = 5,\ 10,\ 15,\ 25$, and 50.

In Fig. 14, we plot the time evolution of the numerical solutions, C and U, with $K = 9,\ R = 11,\ \Delta t = 0.01,\ T = 10$, and $M = 0.002$. As time evolves, concentrations of nutrient C is decreasing and cell density U is increasing.

In Fig. 15, the slice plot around core of scaffolds is depicted. On the middle and the top portion of the third stack, we can check that cell grows more in the top portion. Initially, nutrient concentration profile was uniform and cell seeding was also constant on the first, the third, and the fifth scaffolds. As time evolves, cell consumes the nutrient and grows

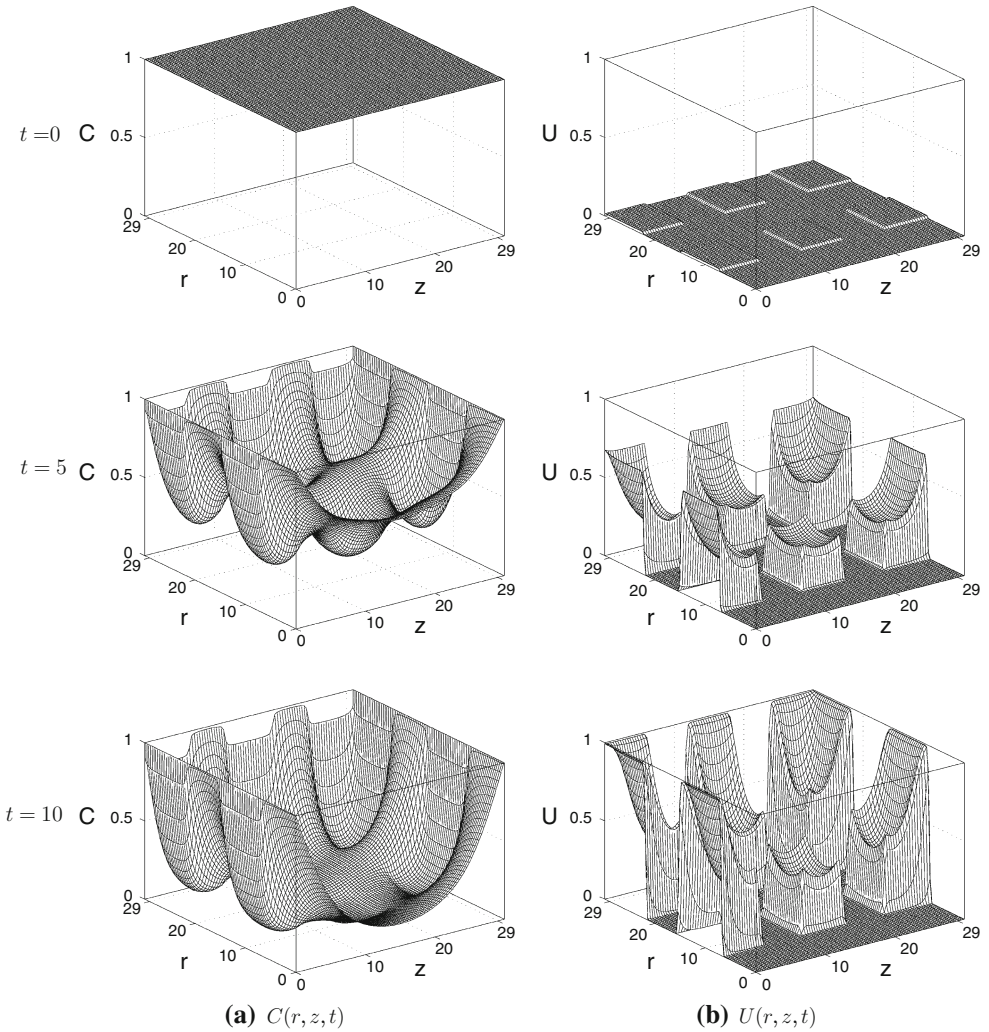

Fig. 17 The time evolution of the numerical solutions on Construct C, **a** C and **b** U with $K = 9.0$, $R = 11.0$, $M = 0.002$, $\Delta t = 0.01$, and 256×256 mesh

uniformly. However, at later time, nonuniform distribution of the nutrient concentration occurs due to the limited diffusion. And this triggers higher cell density along the top portion of the third scaffold.

4.4 Another construct: alternating concentric annulus seeding

We consider another construct, which is an alternating concentric annulus seeding as shown in Fig. 16. For the parameter set, we use $K = 9.0$, $R = 11.0$, $\Delta t = 0.01$, $T = 10$, and $M = 0.002$ with a 256×256 spatial mesh.

In Fig. 17, we plot the time evolution of the numerical solutions with initial condition (Fig. 16) at $T = 10$ with a 128×128 spatial mesh. As time evolves, concentration of nutrients C is decreasing and the cell density U is increasing.

Figure 18 shows comparison between measured cell densities for the third scaffold on construct A and simulated cell densities in construct A and C at $T = 10$. (a) Middle portion (circle markers represent experimental data on Construct A) and (b) top portion (squared markers represent experimental data on Construct A). Error bar represents the standard deviation of the measured cell density. As the alternating concentric annulus seeding supplies enough nutrients into inside scaffolds, the cell density becomes higher in the cell core. This result suggests that we can design cell distribution by changing cell seeding techniques.

5 Conclusions

In this paper, we proposed an efficient and accurate hybrid numerical scheme of a mathematical model to predict the growth and distribution of cells in scaffolds. The numerical algorithm is a hybrid method which uses both finite difference approximations and analytic closed-form solutions.

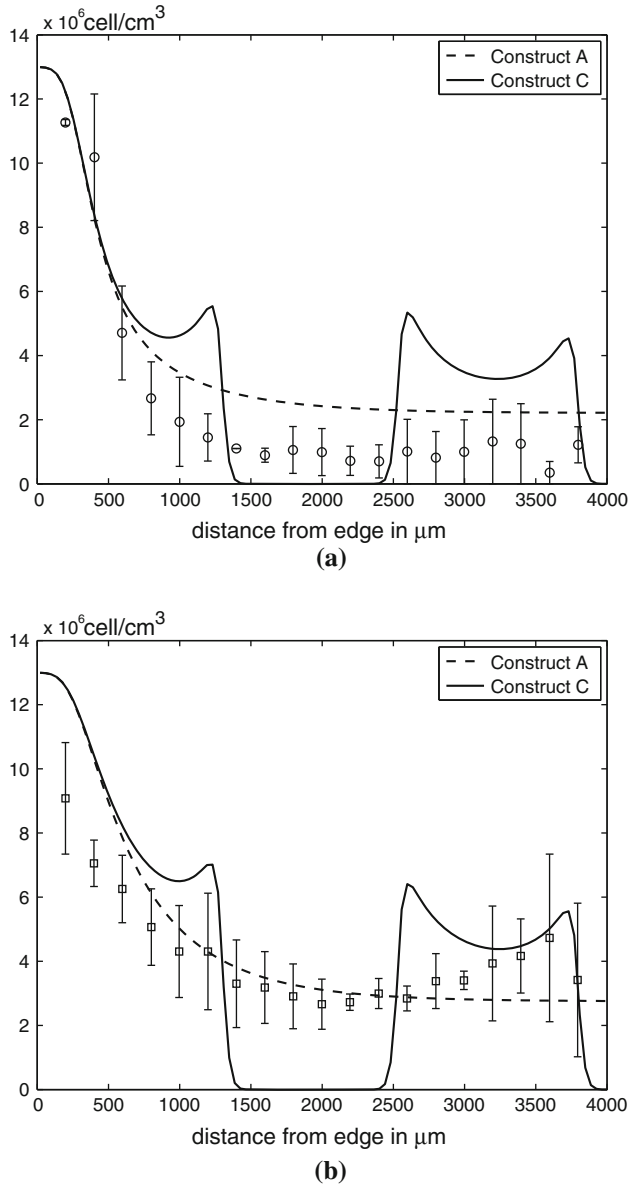

Fig. 18 Measured and simulated cell densities for the third scaffold in construct A and C (alternating concentric annulus seeding) at $T = 10$ with $K = 9.0$, $R = 11.0$, and $M = 0.002$. **a** Middle portion (*circle markers* represent experiment data on Construct A) and **b** top portion (*squared markers* represent experiment data on Construct A). *Error bar* represents the standard deviation of measured cell density

Moreover, we proposed an optimization algorithm which finds the best set of model parameters that minimize a discrete l_2 error between numerical and experimental data. Using the mathematical model and its efficient and accurate numerical simulations, we could interpret experimental results and identify dominating mechanisms. The effects of each model parameter were numerically investigated. As a future work, we plan to incorporate stress effects into the mathematical model since stresses play a role on the cell growth in scaffolds (Correa-Duarte et al. 2004).

Acknowledgments This work was supported by the National Research Foundation of Korea(NRF) grant funded by the Korea government (MEST) (No. 2010-0027813). The authors also thank the anonymous referees for the constructive and helpful comments on the revision of this article.

Conflict of interest None of the authors have financial or personal relationships with other people or organizations that could inappropriately influence or bias the currently presented work.

References

Beaupr GS, Hayes WC (1985) Finite element analysis of a three dimensional open celled model for trabecular bone. J Biomech Eng 107(3):249–256

Bose S, Darsell J, Hosick H, Yang L, Sarkar D, Bandyopadhyay A (2002) Processing and characterization of porous alumina scaffolds. J Mater Sci: Mater Med 13(1):23–28

Briggs WL (1987) A multigrid tutorial. SIAM, Philadelphia

Byrne DP, Lacroix D, Planell JA, Kelly DJ, Prendergast PJ (2007) Simulation of tissue differentiation in a scaffold as a function of porosity, Youngs modulus and dissolution rate: Application of mechanobiological models in tissue engineering. Biomaterials 28(36):5544–5554

Cahill S, Lohfeld S, McHugh PE (2009) Finite element predictions compared to experimental results for the effective modulus of bone tissue engineering scaffolds fabricated by selective laser sintering. J Mater Sci Mater Med 20(6):1255–1262

Correa-Duarte MA, Wagner N, Rojas-Chapana J, Morsczeck C, Thie M, Giersig M (2004) Fabrication and biocompatibility of carbon nanotube-based 3D networks as scaffolds for cell seeding and growth. Nano Lett 4(11):2235–2236

Dunn JCY, Chan WY, Cristini V, Kim JS, Lowengrub J, Singh S, Wu BM (2006) Analysis of cell growth in three-dimensional scaffolds. Tissue Eng 12(4):707–716

Eisenbarth E (2007) Biomaterials for tissue engineering. Adv Eng Mater 9(12):1051–1060

Ermentrout GB, Edelstein-Keshet L (1993) Cellular automata approaches to biological modeling. J Theor Biol 160(1):97–133

Fang Z, Starly B, Sun W (2005) Computer-aided characterization for effective mechanical properties of porous tissue scaffolds. Comput-Aided Des 37(1):65–72

Flaibani M, Magrofuoco E, Elvassore N (2010) Computational modeling of cell growth heterogeneity in a perfused 3D scaffold. Ind Eng Chem Res 49(2):859–869

Fritsch FN, Carlson RE (1980) Monotone piecewise cubic interpolation. SIAM J Numer Anal 17(2):238–246

Galban CJ, Locke BR (1997) Analysis of cell growth in a polymer scaffold using a moving boundary approach. Biotechnol Bioeng 56:422–432

Galban CJ, Locke BR (1999) Effects of spatial variation of cells and nutrient and product coupled with product inhibition on cell growth in a polymer scaffold. Biotechnol Bioeng 64(6):633–643

Hing K, Best S, Bonfield W (1999) Characterization of porous hydroxyapatite. J Mater Sci: Mater Med 10(3):135–145

Hori Y, Inoue S, Hirano Y, Tabata Y (2004) Effect of culture substrates and fibroblast growth factor addition on the proliferation and differentiation of rat bone marrow stromal cells. Tissue Eng 10(7–8):995–1005

Landman KA, Cai AQ (2007) Cell proliferation and oxygen diffusion in a vascularising scaffold. Bull Math Biol 69(7):2405–2428

Langer R, Vacanti JP (1993) Tissue engineering. Science 260:920–926

Lanza R, Langer R, Vacanti JP (2000) Principles of tissue engineering. 2nd ed. Academic Press, New York

Lemon G, King JR, Byrne HM, Jensen OE (2006) Mathematical modelling of engineered tissue growth using a multiphase porous flow mixture theory. J Math Biol 52(5):571–594

Lewis MC, MacArthur BD, Malda J, Pettet G, Please CP (2005) Heterogeneous proliferation within engineered cartilaginous tissue: the role of oxygen tension. Biotechnol Bioeng 91(5):607–615

Li Y, Ma T, Kniss DA, Lasky LC, Yang ST (2001) Effects of filtration seeding on cell density, spatial distribution, and proliferation in nonwoven fibrous matrices. Biotechnol Prog 17(5):935–944

Longo D, Peirce SA, Skalak TC, Davidson L, Marsden M, Dzamba B, DeSimone DW (2004) Multicellular computer simulation of morphogenesis: blastocoel roof thinning and matrix assembly in Xenopus laevis. Dev Biol 271(1):210–222

Malda J, Woodfield TBF, van der Vloodt F, Kooy FK, Martens DE, Tramper J, van der Blitterswijk CA, Riesle J (2004) The effect of PEGT/PBT scaffold architecture on oxygen gradients in tissue engineered cartilaginous constructs. Biomaterials 25(26):5773–5780

Murray JD (2002) Mathematical biology. 3rd edn. Springer, Berlin

Nerem RM, Sambanis A (1995) Tissue engineering: from biology to biological substitutes. Tissue Eng 1(1):3–13

Nishimura I, Garrell RL, Hedrick M, Iida K, Osher S, Wu B (2003) Precursor tissue analogs as a tissue-engineering strategy. Tissue Eng 9(1):77–89

Obradovic B, Meldon JH, Freed LE, Vunjak-Novakovic G (2000) Glycosaminoglycan deposition in engineered cartilage: Experiments and mathematical model. AIChE J 46(9):1860–1871

Patel M, Fisher JP (2008) Biomaterial scaffolds in pediatric tissue engineering. Pediatr Res 63(5):497–501

Pisu M, Lai N, Cinotti A, Alessandro C, Cao G (2004) Modeling of engineered cartilage growth in rotating bioreactors. Chem Eng Sci 59(22–23):5035–5040

Skalak R, Fox CF (1988) Tissue engineering. Alan R Liss Prepace, New York

Stuart A, Humphries AR (1998) Dynamical system and numerical analysis. Cambridge University Press, Cambridge

Trottenberg U, Oosterlee C, Schüller A (2001) Multigrid. Academic Press, New York

Williams JL, Lewis JL (1982) Properties and an anisotropic model of cancellous bone from the proximal tibia epiphysis. J Biomech Eng 104(1):50–56

Yang S, Leong KF, Du Z, Chua C-K (2001a) The design of scaffolds for use in tissue engineering. Part I. Traditional factors. Tissue Eng 7(6):679–689

Yang TH, Miyoshi H, Ohshima N (2001b) Novel cell immobilization method utilizing centrifugal force to achieve high-density hepatocylte culture in porous scaffold. J Biomed Mater Res 55(3):379–386